Journal of Molecular Spectroscopy 257 (2009) 57–65

Contents lists available at ScienceDirect

Journal of Molecular Spectroscopy

journal homepage: www.elsevier.com/locate/jms

An *ab initio* calculation of the vibrational energies and transition moments of HSOH

Sergei N. Yurchenko [a], Andrey Yachmenev [b], Walter Thiel [b], Oliver Baum [c], Thomas F. Giesen [c], Vladlen V. Melnikov [d,1], Per Jensen [d,*]

[a] *Institut für Physikalische Chemie und Elektrochemie, TU Dresden, D-01062 Dresden, Germany*
[b] *Max-Planck-Institut für Kohlenforschung, Kaiser-Wilhelm-Platz 1, D-45470 Mülheim an der Ruhr, Germany*
[c] *I. Physikalisches Institut, Universität zu Köln, Zülpicher Straße 77, D-50937 Köln, Germany*
[d] *FB C – Physikalische und Theoretische Chemie, Bergische Universität, D-42097 Wuppertal, Germany*

ARTICLE INFO

Article history:
Received 27 May 2009
In revised form 19 June 2009
Available online 28 June 2009

Keywords:
HSOH
Oxadisulfane
ab initio
Potential energy surface
Dipole moment surface
Vibrational energies
Vibrational transition moments
TROVE

ABSTRACT

We report new *ab initio* potential energy and dipole moment surfaces for the electronic ground state of HSOH, calculated by the CCSD(T) method (coupled cluster theory with single and double substitutions and a perturbative treatment of connected triple excitations) with augmented correlation-consistent basis sets up to quadruple-zeta quality, aug-cc-pV(Q+*d*)Z. The energy range covered extends up to 20 000 cm^{-1} above equilibrium. Parameterized analytical functions have been fitted through the *ab initio* points. Based on the analytical potential energy and dipole moment surfaces obtained, vibrational term values and transition moments have been calculated by means of the variational program TROVE. The theoretical term values for the fundamental levels ν_{SH} (SH-stretch) and ν_{OH} (OH-stretch), the intensity ratio of the corresponding fundamental bands, and the torsional splitting in the vibrational ground state are in good agreement with experiment. This is evidence for the high quality of the potential energy surface. The theoretical results underline the importance of vibrational averaging, and they allow us to explain extensive perturbations recently found experimentally in the SH-stretch fundamental band of HSOH.

1. Introduction

After the first spectroscopic characterization of oxadisulfane HSOH as recently as in 2003 [1], this molecule (and its deuterated isotopologues DSOD and HSOD) has received substantial experimental and theoretical attention [2–11] as the 'long-missing link' between the better known molecules HOOH and HSSH. Each of the three molecules HOOH, HSSH, and HSOH has a skew-chain equilibrium geometry, and particularly interesting features of their spectra originate in the energy splittings resulting from the internal rotation, or torsion, of the OH or SH moieties around the axis connecting the two heavy atoms (we denote this axis as the *z* axis; see Section 3.2 below). The torsional motion couples significantly with the over-all rotation of the molecule about the *z* axis and, in consequence, the torsional splittings depend strongly on the rotational excitation, in particular on the quantum number K_a which is the absolute value of the projection, in units of ħ, of the total angular momentum onto the *z* axis. It is well known that in HOOH and HSSH, the torsional splittings 'stagger' with K_a so that, for example, states with even (odd) K_a values have larger (smaller) splittings. For HSOH, a more complicated variation of the splittings with K_a was observed experimentally [1,3]; it has an approximate periodicity with a period of three K_a-values. Initially, the unexpected splitting pattern was explained in terms of a semi-empirical model [3] based on ideas of Hougen [12] (see also Ref. [13]). The periodicity of three K_a-values in the torsional splittings was found to derive from the fact that the moments of inertia of the OH and SH moieties with respect to the *z* axis form a ratio of about 2:1; for HOOH and HSSH a periodicity of two K_a-values ensues because for these molecules, the analogous ratio is 1:1.

Quite recently [11], a slightly extended version of the Hougen-type model from Ref. [3] has been used for a successful analysis of all torsional splittings observed experimentally for HSOH. The values of the splittings were least-squares fitted to parameterized expressions derived from the model. In parallel, we have given an equally successful explanation [9] of the observed splittings using an alternative, first-principles approach in which the splittings are calculated directly from an *ab initio* potential energy surface (PES) by means of the program system TROVE [14] (Theoretical Rotation–Vibration Energies). TROVE can, in principle, calculate the rotation–vibration energies of any polyatomic molecule in an isolated electronic state, and the generally high accuracy of the rotation–vibration energies obtained has already been demonstrated in Ref. [14]. In the variational solution of the rotation–vibration Schrödinger equation for HSOH [9] we used

* Corresponding author. Fax: +49 202 439 2509.
E-mail address: jensen@uni-wuppertal.de (P. Jensen).
[1] Present address: Siberian Physical-technical Institute, Tomsk State University, Tomsk, 634050 Russia.

0022-2852/$ - see front matter © 2009 Elsevier Inc. All rights reserved.
doi:10.1016/j.jms.2009.06.010

the Hougen–Bunker–Johns (HBJ) nonrigid-reference configuration method [15]. In this method the reference geometry is chosen to minimize the vibration–torsion coupling in the kinetic energy operator. In the calculation of HSOH torsional splittings in Ref. [9] we also explored an alternative approach, akin to the semirigid bender model by Bunker and Landsberg [16], where the geometries along the torsional minimum energy path (i.e., a path where, as the torsional motion takes place, all other structural parameters than the torsional coordinate relax to minimize the potential energy) are taken as the reference configuration. In this case, the torsion–vibration coupling is minimized in the PES. It turned out that this approach provides very accurate torsional splittings as well as quite accurate values for the torsion-rotation term values.

In the present work, we describe the *ab initio* PES for the electronic ground state of HSOH, computed by the CCSD(T) *ab initio* method, which served as starting point for the calculation of the torsional splittings in Ref. [9]. Furthermore, we report the computation of an accompanying CCSD(T) *ab initio* dipole moment surface (DMS). For both the PES and the DMS, we have constructed suitable analytical-function representations of the *ab initio* points and we use these analytical representations as input for the TROVE program to calculate vibrational term values and vibrational transition moments for selected vibrational bands of HSOH.

The parameterized analytical representation of the PES has been constructed by least-squares fitting to two sets of *ab initio* energies [see Section 3 below]. One set, comprising 105 000 data points, was calculated with the aug-cc-pVTZ basis set and the other set, comprising 10 168 data points, was calculated with the aug-cc-pV(Q+*d*)Z basis set. The 10 168 geometries in the second set of data points were selected to cover in detail the energy range up to 20 000 cm^{-1} above equilibrium. The analytical function representing the PES is defined in terms of 762 parameter values.

The *ab initio* dipole moment data points were computed at the CCSD(T)/aug-cc-pV(T+*d*)Z level of theory for 8936 geometries. The finite difference scheme was employed for the dipole moment calculation. The analytical functions representing the DMS components μ_x, μ_y, and μ_z [see Section 3.2 for the definition of the *xyz* axis system] are defined in terms of 428, 382, and 420 parameter values, respectively.

The *ab initio* study of the present work is the most complete and accurate reported thus far. We have already validated the *ab initio* PES in Ref. [9] by showing that the torsional splittings and the torsion–rotation term values obtained from the PES are in excellent agreement with the available experimental values [1,3,8,11]. In the present work, we extend this validation by comparing also the remaining, experimentally available term values associated with the OH-stretch [7] and SH-stretch [7,10] fundamental levels.

The paper is structured as follows. In Section 2, we describe the *ab initio* methods employed for the electronic structure calculations. We also define in this section the grids of nuclear geometries, at which *ab initio* energies were calculated, and characterize the computed potential energy and dipole moment surfaces of HSOH. The analytical representations of the PES and DMS are introduced in Section 3. The variational nuclear-motion calculations are reported in Section 4 together with the computed theoretical values for the vibrational term values and transition moments of HSOH. In Section 5, we discuss the theoretical description of the OH-stretch and SH-stretch fundamental levels v_{OH} and v_{SH} while comparing the theoretical results with the experimental findings. Finally, Section 6 offers additional discussion and some conclusions.

2. *Ab initio* calculations

The *ab initio* calculations of the present work have been made with the MOLPRO2002 package [17,18], employing the CCSD(T) (coupled cluster theory with all single and double substitutions from the Hartree–Fock reference determinant [19] augmented by a perturbative treatment of connected triple excitations [20,21]) method.

2.1. Potential energy surface

The CCSD(T) energy calculations have been carried out in the frozen-core approximation with three different combinations of basis sets: (a) aug-cc-pVDZ basis sets for H, O, and S; (b) aug-cc-pVTZ basis sets for H, O, and S; and (c) cc-pVQZ, aug-cc-pVQZ, and aug-cc-pV(Q+*d*)Z basis sets for H, O, and S, respectively [22–25]. In the largest basis set (c), we adopt the *d*-corrected basis for S from Wilson and Dunning [25], and we do not augment the cc-pVQZ basis for H since we do not expect the corresponding diffuse functions to play a significant role. The basis set combinations (a), (b), and (c) are referred to as ADZ, ATZ, and A(Q+*d*)Z, respectively.

The CCSD(T) calculations with the three basis sets ADZ, ATZ, and A(Q+*d*)Z have very different computer-resource requirements. We used the relatively modest level of theory associated with the ADZ basis set for a preliminary scan of the PES and computed about a million *ab initio* points on a regular 6D grid. This provided us with a very detailed, albeit qualitative, survey of the PES and made it possible to determine the range of geometries necessary to describe the PES of HSOH up to 20 000 cm^{-1} above equilibrium. Exploring the potential energy surface further we have computed about 105 000 energies at the ATZ level of *ab initio* theory, covering the energy range up to 20 000 cm^{-1} above equilibrium. This strategy for choosing the grid of geometries is similar to that used in Ref. [26]. Then, finally, we run more expensive A(Q+*d*)Z calculations at 10 168 geometries. Because of the high computational demands at the A(Q+*d*)Z level of theory, it was especially important to select appropriate molecular geometries for the A(Q+*d*)Z calculations from the results of the lower-level calculations.

In order to describe the geometry of HSOH we introduce six internal coordinates: The S–O distance r_{SO}, the S–H distance r_{SH}, the O–H distance r_{OH}, $\alpha_{HOS} = \angle(H–O–S) \in [0,\pi]$, $\alpha_{OSH} = \angle(O–S–H) \in [0,\pi]$, and the torsional angle $\tau_{HSOH} \in [0,2\pi]$ (the dihedral angle between the HOS and OSH planes). Fig. 1 shows six one-dimensional (1D) cuts through the PES, visualizing the variation of the PES with each of these coordinates. In each case, the five remaining coordinates are set equal to their equilibrium values.

The equilibrium values of r_{SO}, r_{SH}, r_{OH}, α_{HOS}, α_{OSH}, and τ_{HSOH} are listed in Table 1 and compared with CCSD(T)/cc-pCVQZ values from Ref. [1], with very recent CCSD(T,full)/cc-pwCVQZ *ab initio* results by Denis [27] and with the empirical structural parameters derived by Baum et al. [5]. The table also gives the calculated *cis* and *trans* barriers to torsional motion; these values are compared with the CCSD(T)/cc-pCVQZ values from Ref. [1] and with MP2/aug-cc-pVTZ values from Ref. [28]. The top of the *cis*(*trans*) barrier is the maximum obtained for $\tau_{HSOH} = 0°$ (180°) and all other structural parameters relaxed to minimize the potential energy.

We have also computed the barrier values corresponding to a path between the two equivalent minima of the PES where one of the angles α_{HOS} or α_{OSH} reaches 180° (that is, either the HOS moiety or the OSH moiety becomes linear). We find these barriers at the MP2/aug-cc-pV(T+*d*)Z level of theory by using constrained optimization. The barrier for $\alpha_{HOS} = 180°$ is 11 780 cm^{-1}, while the barrier for $\alpha_{OSH} = 180°$ is much higher, 37 524 cm^{-1} (see Fig. 1). The lowest-energy linear configuration of the molecule is found approximately 55 424 cm^{-1} above equilibrium at the MP2/aug-cc-pV(T+*d*)Z level of theory.

2.2. Dipole moment surfaces

The *ab initio* dipole moment values were computed with MOLPRO2002 at the CCSD(T)/A(T+*d*)Z level of theory [19–25] in

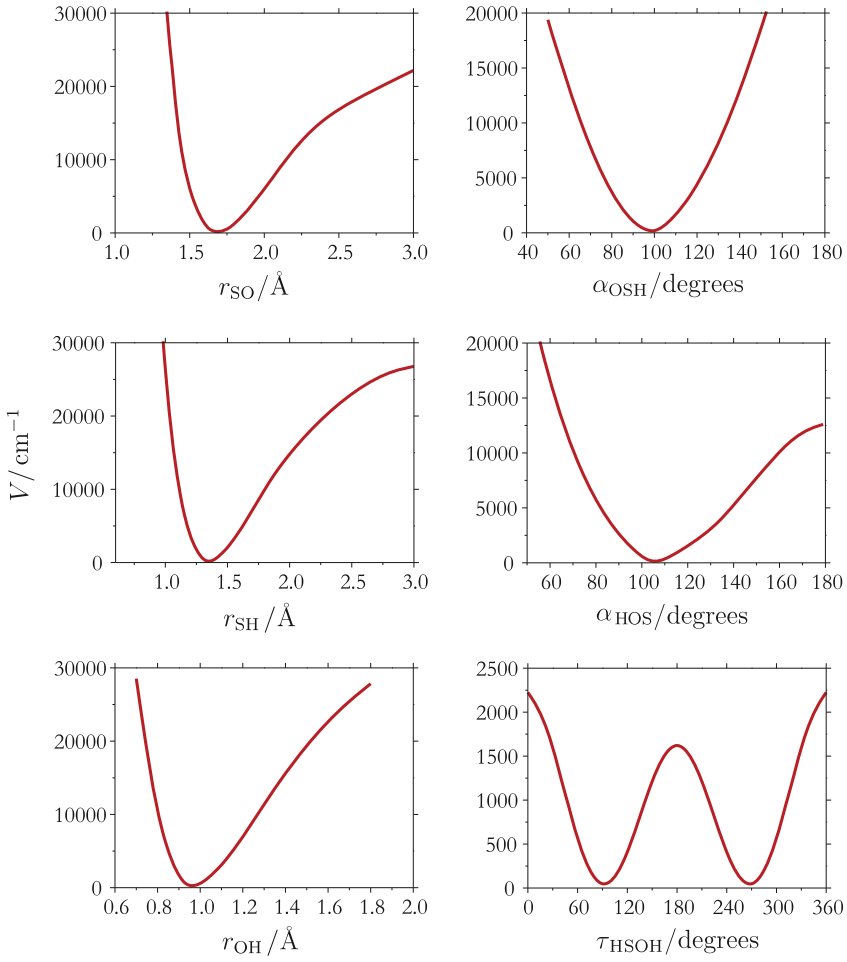

Fig. 1. Six one-dimensional (1D) cuts through the potential energy function for HSOH (one for each degree of freedom) with the remaining five coordinates taken at their equilibrium values.

Table 1
Equilibrium and transition geometries of HSOH.

	Equilibrium geometry				Transition states[a]	
	A(Q+*d*)Z[a]	Ref. [1][b]	Ref. [27][c]	Ref. [5][d]	*cis*	*trans*
r_{SO} (Å)	1.66725	1.6616	1.6614	1.6616(1)	1.687	1.690
r_{SH} (Å)	1.34431	1.3414	1.3413	1.3420(2)	1.341	1.337
r_{OH} (Å)	0.96178	0.9601	0.9601	0.9606(3)	0.960	0.962
α_{HOS} (°)	107.141	107.01	107.0	107.19(3)	108.911	105.564
α_{OSH} (°)	98.424	98.55	98.6	98.57(5)	99.411	93.325
τ_{HSOH} (°)	91.431	91.29	91.3	90.41(11)	0	180
V_{opt} (cm^{-1})					2163.3[e]	1520.9[f]

[a] Present work, obtained by geometry optimization carried out with MOLPRO2002 [17,18].
[b] CCSD(T)/cc-pCVQZ *ab initio*.
[c] CCSD(T,full)/cc-pwCVQZ *ab initio*; see Ref. [27] for further details.
[d] Empirical equilibrium geometry derived from experimental values of A_0, B_0, and C_0 in conjunction with CCSD(T)/cc-pCVQZ *ab initio* values of the α_r constants for HSOH, H^{34}SOH, HSOD, and DSOD. See Ref. [5] for details. Numbers in parentheses are quoted uncertainties in units of the last digit.
[e] *cis*-barrier for torsional motion. The CCSD(T)/cc-pCVQZ value from Ref. [1] is 2216 cm^{-1} and the aug-cc-pVTZ/MP2 value from Ref. [28] is 2164 cm^{-1}.
[f] *trans*-barrier for torsional motion. The CCSD(T)/cc-pCVQZ value from Ref. [1] is 1579 cm^{-1} and the aug-cc-pVTZ/MP2 value from Ref. [28] is 1473.5 cm^{-1}.

the frozen-core approximation. For these calculations we selected 8936 geometries with energies less than 12 000 cm^{-1} above equilibrium. The dipole moment components along the molecule-fixed axes were obtained as derivatives of the electronic energy with respect to the components of an external electric field. The field derivatives were computed for each geometry by means of the central finite difference scheme; for each of the *x*, *y*, and *z* molecule-fixed axes, the molecule was subjected to external electric fields with components of +0.005 a.u. and −0.005 a.u., respectively, along the axis in question.

3. Fitting of the surfaces

3.1. Potential energy surface

Fig. 1 shows that the vibrational modes of HSOH, with the exception of the torsional mode, can be viewed as oscillations around a single minimum on the PES. The torsional motion, on the other hand, involves tunneling between two equivalent minima on the PES through the *cis* and *trans* barriers whose heights are given in Table 1. We employ a cosine-type expansion to repre-

sent the dependence of the PES on the torsional angle τ_{HSOH}. We choose this expansion with a view to the fact that the PES is invariant under the inversion operation E^* [29] which causes the coordinate change $\tau_{HSOH} \to 2\pi - \tau_{HSOH}$. The dependence of the PES on the three stretching coordinates is described by expansions in Morse-type variables $y = 1 - \exp(-a[r - r_e])$, while for the bending coordinates we use the displacements $\Delta\alpha = \alpha - \alpha_e$. The expansion of the PES thus becomes

$$\begin{aligned} V(\xi_{OH}, \xi_{OS}, \xi_{SH}, \xi_{HOS}, \xi_{OSH}, \xi_{HSOH}) &= V_e + \sum_j F_j \xi_j + \sum_{j\leqslant k} F_{jk} \xi_j \xi_k + \sum_{j\leqslant k\leqslant l} F_{jkl} \xi_j \xi_k \xi_l \\ &+ \sum_{j\leqslant k\leqslant l\leqslant m} F_{jklm} \xi_j \xi_k \xi_l \xi_m + \sum_{j\leqslant k\leqslant l\leqslant m\leqslant n} F_{jklmn} \xi_j \xi_k \xi_l \xi_m \xi_n \\ &+ \sum_{j\leqslant k\leqslant l\leqslant m\leqslant n\leqslant o} F_{jklmno} \xi_j \xi_k \xi_l \xi_m \xi_n \xi_o \end{aligned} \quad (1)$$

The expansion variables are

$$\xi_k = 1 - \exp(-a_k(r_k - r_k^{ref})), \quad k = SO, SH, \text{or } OH \quad (2)$$

$$\xi_{HOS} = \alpha_{HOS} - \alpha_{HOS}^{ref}, \quad (3)$$

$$\xi_{OSH} = \alpha_{OSH} - \alpha_{OSH}^{ref}, \quad (4)$$

$$\xi_{HSOH} = \cos\tau_{HSOH} - \cos\tau_{HSOH}^{ref}, \quad (5)$$

where r_k^{ref} and α_k^{ref} are reference values of the structural parameters, the a_k are molecular parameters, V_e is the value of the PES at equilibrium, and the quantities $F_{jk\ldots}$ are the expansion coefficients. Since $\cos(2\pi - \tau_{HSOH}) = \cos\tau_{HSOH}$, the function in Eq. (1) automatically satisfies the symmetry requirement mentioned above so that there are no symmetry relations between the potential parameters, i.e., all $F_{jk\ldots}$ are independent. We take the reference values as $r_{SO}^{ref} = 1.69031$ Å, $r_{SH}^{ref} = 1.33653$ Å, $r_{OH}^{ref} = 0.96229$ Å, $\alpha_{HOS}^{ref} = 105.56^\circ$, $\alpha_{OSH}^{ref} = 93.32^\circ$, and $\tau_{HSOH}^{ref} = 180^\circ$.

Our highest-quality *ab initio* surface A(Q+*d*)Z is based on 10168 *ab initio* points covering, for the most part, the region below 12000 cm^{-1}. That is, the highest-quality *ab initio* points cover a limited region of configuration space. The less accurate ATZ PES covers in great detail the region up to 20000 cm^{-1} with almost 105000 points. In order to prevent the fitted, analytical PES from having a significantly wrong behavior in regions of configuration space not sampled by the A(Q+*d*)Z data points, we use both the ATZ and the A(Q+*d*)Z data sets as input for the least-squares fitting producing the optimized values of the potential energy parameters $F_{jkl\ldots}$. In this fitting, the points in the large ATZ data set are given weight factors typically 10^4 times smaller than those of the A(Q+*d*)Z data points. In this way the geometries, for which A(Q+*d*)Z *ab initio* energies exist, are greatly favored because of the large weight factors. However outside the A(Q+*d*)Z grid the fit is controlled by the points of the vast data set ATZ. The ratio of 10^4 between the weight factors used for the A(Q+*d*)Z and ATZ points was found by numerical experiments. We needed 762 fitting parameters to reproduce the A(Q+*d*)Z electronic energies with the root-mean-square (rms) error of 2.8 cm^{-1}. The analytical PES obtained by combination of the ATZ and A(Q+*d*)Z *ab initio* data sets is denoted A(Q+*d*)Z*. This analytical PES is assumed to be of A(Q+*d*)Z quality in the lower energy region up to 12000 cm^{-1} above equilibrium (since this is where the A(Q+*d*)Z *ab initio* data exist) and to have a qualitative correct behavior, at least of ATZ quality, at higher energy up to 20000 cm^{-1}.

In order to establish the quality of the ATZ *ab initio* energies, we have also fitted the 105000 ATZ data points without the A(Q+*d*)Z points. In this fitting, we could usefully vary 898 parameters that describe the ATZ energies with rms errors of 4.4 cm^{-1}, 13 cm^{-1}, and 32 cm^{-1} below 10000 cm^{-1}, 15000 cm^{-1}, and 20000 cm^{-1}, respectively.

The *ab initio* energy values and the parameter values obtained from the fits of the potential energy function in Eq. (1) are available as Supplementary material together with FORTRAN routines for evaluating the corresponding potential energy values at arbitrary geometries. The A(Q+*d*)Z* potential energy surface, obtained by combination of the ATZ and A(Q+*d*)Z *ab initio* data sets as described above, is expected to provide a good description of the electronic ground state of HSOH at energies up to 20000 cm^{-1} above equilibrium.

3.2. Dipole moment surfaces

Towards obtaining analytical representations of the electronically averaged dipole moment components for HSOH we introduced an axis system as follows. The *z* axis is aligned along the SO bond, pointing from S to O, and the *x* axis lies in the plane containing the SO and SH bonds and is oriented such that the H nucleus in the SH moiety has a positive *x* value. The *y* axis is oriented such that the *xyz* axis system is right-handed. This *xyz* axes are not exactly principal axes, but the *xyz* axis system is close to the principal axis system *abc* shown in Fig. 2 with the *z* axis being close to the *a* axis which has the smallest moment of inertia. With the chosen axes, the *y* component of the dipole moment is antisymmetric with respect to inversion E^* [29] (that is, it has A'' symmetry in the $\mathbf{C}_s$(M) group [29]), while the *x* and *z* component are totally symmetric (i.e., they have A' symmetry). The three dipole components are represented by the following analytical functions:

$$\begin{aligned} \bar{\mu}_\alpha(\zeta_{OH}, \zeta_{SO}, \zeta_{SH}, \zeta_{HOS}, \zeta_{OSH}, \zeta_{HSOH}) &= \mu_0^{(\alpha)} + \sum_j \mu_j^{(\alpha)} \zeta_j + \sum_{j\leqslant k} \mu_{jk}^{(\alpha)} \zeta_j \zeta_k + \sum_{j\leqslant k\leqslant l} \mu_{jkl}^{(\alpha)} \zeta_j \zeta_k \zeta_l \\ &+ \sum_{j\leqslant k\leqslant l\leqslant m} \mu_{jklm}^{(\alpha)} \zeta_j \zeta_k \zeta_l \zeta_m \end{aligned} \quad (6)$$

with $\alpha = x$ or *z*, and

$$\begin{aligned} \bar{\mu}_y(\zeta_{OH}, \zeta_{SO}, \zeta_{SH}, \zeta_{HOS}, \zeta_{OSH}, \zeta_{HSOH}) &= \sin\tau_{HSOH} \left[\mu_0^{(y)} + \sum_j \mu_j^{(y)} \zeta_j + \sum_{j\leqslant k} \mu_{jk}^{(y)} \zeta_j \zeta_k + \sum_{j\leqslant k\leqslant l} \mu_{jkl}^{(y)} \zeta_j \zeta_k \zeta_l \right. \\ &\left. + \sum_{j\leqslant k\leqslant l\leqslant m} \mu_{jklm}^{(y)} \zeta_j \zeta_k \zeta_l \zeta_m \right]. \end{aligned} \quad (7)$$

The dipole moment components are expanded in the variables

$$\zeta_k = r_k - r_k^{ref}, \quad k = OH, SO, \text{or } SH, \quad (8)$$

$\zeta_{HOS} = \xi_{HOS}$, $\zeta_{OSH} = \xi_{OSH}$, and $\zeta_{HSOH} = \xi_{HSOH}$, where ξ_{HOS}, ξ_{OSH}, and ξ_{HSOH} are given in Eqs. (3)–(5).

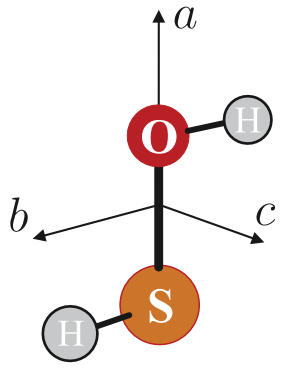

Fig. 2. The *abc* axes for the HSOH molecule.

We have determined the values of the expansion parameters of Eqs. (6) and (7) in three least-squares fittings, each of them to 8936 *ab initio* dipole moment components $\bar{\mu}_\alpha$, $\alpha = x,y,z$. In the three final fittings, we could usefully vary 428 ($\bar{\mu}_x$), 382 ($\bar{\mu}_y$), and 420 ($\bar{\mu}_z$) parameters, obtaining rms deviations of 0.0022, 0.0023, and 0.0149 D, respectively. In the lower energy region (below 8000 cm^{-1}) these deviations are smaller, 0.0005, 0.0004, and 0.0016 D, respectively. The optimized parameters are given as Supplementary material together with a FORTRAN routine for calculating the dipole moment values from Eqs. (6) and (7). We refer to the level of theory used for computing the electric dipole moment as A(T+*d*)Z.

For comparison with experimentally derived dipole moments, we must transform the dipole moment so as to obtain the components $\bar{\mu}_a, \bar{\mu}_b$, and $\bar{\mu}_c$ along the principal axes *abc* shown in Fig. 2. The dependence of $\bar{\mu}_a, \bar{\mu}_b$, and $\bar{\mu}_c$ for HSOH on the torsional angle τ_{HSOH} is depicted in Fig. 3, where we plot the dipole moment components obtained when the values of the structural parameters r_{SO}, r_{SH}, r_{OH}, α_{HOS}, α_{OSH} are determined by the torsional minimum energy path geometries of HSOH [9]. For the equilibrium values of the *ab initio* dipole moment we obtain $\bar{\mu}_a = 0.053$D, $\bar{\mu}_b = 0.744$D, and $\bar{\mu}_c = 1.399$D. These values can be compared to the corresponding CCSD(T)/cc-pCVQZ values of 0.0441, 0.7729, and 1.4329 D from Ref. [1]. The component $\bar{\mu}_a$ is close to zero for all torsional angles due to cancellation between the contributions from the SO bond dipole and the sulfur lone pairs. The two components $\bar{\mu}_b$ and $\bar{\mu}_c$ from Fig. 3 vary strongly with τ_{HSOH} and, because of this, the vibrational transition moments (see below) resulting from these components are very different from the corresponding equilibrium dipole moment values.

4. Variational calculations: vibrational term values and transition moments of HSOH

As outlined in Section 1, we employ for the variational calculations the newly developed program TROVE [14]. TROVE is a program suite designed for calculating the rotation–vibration energies of an arbitrary polyatomic molecule in an isolated electronic state. We intend TROVE to be a 'universal black-box' which anyone can use for rotation–vibration calculations. The calculation is variational in that the rotation–vibration Schrödinger equation is solved by numerical diagonalization of a matrix representation of the rotation–vibration Hamiltonian, constructed in terms of a suitable basis set. We describe the rotation–vibration motion of HSOH by means of Hougen–Bunker–Johns (HBJ) theory [15]. That is, we introduce a flexible reference configuration that follows the torsional motion and is defined in terms of the torsional coordinate τ_{HSOH}. The remaining vibrations are viewed as displacements from the reference configuration; they are described by linearized coordinates r^ℓ_{SO}, r^ℓ_{SH}, r^ℓ_{OH}, α^ℓ_{HOS}, and α^ℓ_{OSH}. The linearized coordinate [29] ξ^ℓ coincides with the corresponding geometrically defined coordinate ξ(=r_{SO}, r_{SH}, r_{OH}, α_{HOS}, or α_{OSH}) in the linear approximation. TROVE uses kinetic and potential energy operators expanded as Taylor series about the reference configuration: The kinetic energy is expanded in terms of the ξ^ℓ_k coordinates, and the potential energy is expanded in terms of quantities y^ℓ_k where $y^\ell_k = 1 - \exp(-a_k[\xi^\ell_k - r^e_k])$ with a_k from Eq. (2) for k = SO, SH, or OH, while $y^\ell_k = \xi^\ell_k - \alpha^e_k$ for k = HOS or OSH. The expansions of the kinetic and potential energy operators are truncated after the fourth and eighth order terms, respectively, and test calculations have shown that with these truncations, the energies calculated in the present work are converged to better than 0.05 cm^{-1}.

The vibrational basis set functions are constructed from one-dimensional functions obtained by numerically solving the corresponding one-dimensional (1D) Schrödinger problems by means of the Numerov–Cooley method [14,30]. That is, a vibrational basis function is given as a product of six 1D functions

$$|\phi_{vib}\rangle = |v_{SO}\rangle\,|v_{SH}\rangle\,|v_{OH}\rangle\,|v_{HOS}\rangle\,|v_{OSH}\rangle\,|v_{HSOH}, \tau_{tor}\rangle, \tag{9}$$

where v_X is the principal quantum number for the vibrational mode v_X with X = SO, SH, OH, HOS, and OSH, v_{HSOH} is the principal torsional quantum number, and τ_{tor} = 0 or 1 determines the torsional parity [29] as $(-1)^{\tau_{tor}}$. The quantum numbers v_X are limited as follows: $v_{SO} \leqslant 16$, $v_{SH} \leqslant 8$, $v_{OH} \leqslant 8$, $v_{OSH} \leqslant 8$, $v_{HOS} \leqslant 8$, and $v_{HSOH} \leqslant 18$. The total basis set is also truncated by the energy cutoff E^{cutoff} = 19000 cm^{-1}. That is, in setting up the Hamiltonian matrix, we use only those basis function products in Eq. (9) for which $E_{SO}(v_{SO}) + E_{SH}(v_{SH}) + E_{OH}(v_{OH}) + E_{HOS}(v_{HOS}) + E_{OSH}(v_{OSH}) + E^{(\tau_{tor})}_{HOSH}(v_{HOSH}) \leqslant E^{cutoff}$ [14]. Here, $E_X(v_X)$ is the 1D eigenenergy associated with the wavefunction $|v_X\rangle$ (where X = SO, SH, OH, HOS, OSH); this energy is obtained in the Numerov–Cooley integration. Furthermore, $E^{(\tau_{tor})}_{HOSH}(v_{HOSH})$ is the 1D eigenenergy corresponding to the wavefunction $|v_{HSOH},\tau_{tor}\rangle$. The 1D functions $|v_{SO}\rangle$, $|v_{SH}\rangle$, $|v_{OH}\rangle$, $|v_{HOS}\rangle$, and $|v_{OSH}\rangle$ are all totally symmetric (*i.e.*, of A' symmetry) in $\mathbf{C}_s$(M) [29], whereas $|v_{HSOH},\tau_{tor}\rangle$ has A' (A'') symmetry for τ_{tor} = 0(1). In consequence, the vibrational basis function $|\phi_{vib}\rangle$ in Eq. (9) has A' (A'') symmetry for τ_{tor} = 0(1), and the matrix representation of the vibrational Hamiltonian (*i.e.*, the matrix obtained for J = 0) is block diagonal in τ_{tor}. Thus, for J = 0 we diagonalize two matrix blocks with dimensions 16359 and 14716, respectively, one corresponding to each of the two irreducible representations A' and A'' of $\mathbf{C}_s$(M) [29].

The calculated term values for the fundamental levels v_k and the corresponding values for the torsional splitting are listed in Table 2 and compared to the experimental values available and to other theoretical values. As Supplementary material, we give a more extensive list of term values. The A(Q+*d*)Z* theoretical term value for the OH-stretch fundamental level deviates by only 0.3 cm^{-1} from the experimental gas phase value [7]. For the SH stretching motion, the analogous deviation is larger (6.4 cm^{-1}) which may partly be attributed to the strong interaction between the SH-stretching mode and the torsional mode as discussed in more detail in Section 5 below.

For the OH-stretch term value, the agreement with gas-phase experiment has improved significantly relative to the cc-pVQZ [6] and cc-pV(T+*d*)Z [27] theoretical predictions (Table 2). For the SH-stretch term value, however, it is the other way around; the cc-pVQZ [6] and cc-pV(T+*d*)Z [27] values are in better agreement with experiment than the new A(Q+*d*)Z* value. For the HOS bend, the SO stretch, and the torsion, the theoretical values from the present work are very close to the matrix values [6].

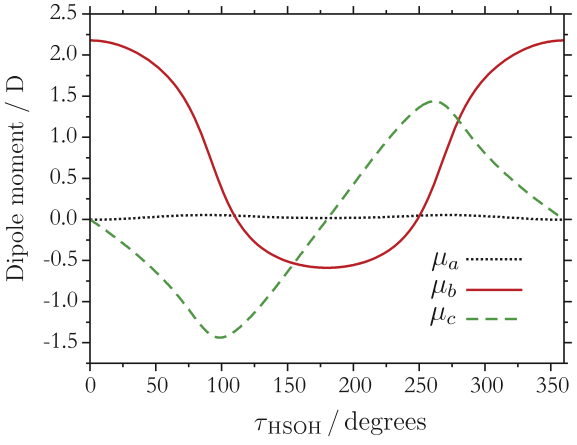

Fig. 3. Dipole moment components for HSOH, computed at the torsional minimum energy path geometries shown in Fig. 1 of Ref. [9].

Table 2
Vibrational term values, torsional splittings (in cm^{-1}) and relative band intensities for the vibrational ground state and the fundamental levels in the electronic ground state of HSOH.

State	Theory			Experiment	
	A(Q+*d*)Z*[a]	cc-pVQZ[b]	cc-pV(T+*d*)Z[c]	Gas-phase[d]	Ar matrix[e]
Vibrational term values					
ν_{OH}	3625.9	3657.2	3640	3625.59260(20)[f]	3608.3
ν_{SH}	2544.4	2536.9	2537	2537.9869(12)[g]	2550.1
ν_{HOS}	1174.0	1188.1	1192		1175.7
ν_{OSH}	1007.7	1004.6	1008		
ν_{SO}	760.0	756.7	760		762.5
ν_{HSOH}	443.0	451.7	457		445.3
State	Theory			Experiment	
	A(Q+*d*)Z*[a]	MP2/cc-pVTZ[h]		Gas-phase[d]	
Torsional splittings					
g.s.	0.00215	0.002339		0.00214[i]	
ν_{OH}	0.0036	0.002177		<0.01[f]	
ν_{SH}	−0.0775	0.001672		0.042(2)[g]	
ν_{HOS}	−0.0335	0.001849			
ν_{OSH}	0.0255	0.002995			
ν_{SO}	0.0546	0.002553			
ν_{HSOH}	0.1279	0.1473			
Band	Theory			Experiment	
	A(Q+*d*)Z*[j]	cc-pVQZ[k]	cc-pV(T+*d*)Z[l]	Ar matrix[e]	
Relative band intensities					
ν_{OH}	16	92	92	43	
ν_{SH}	4	22	21	8	
ν_{HOS}	13	54	55	53	
ν_{OSH}	0	3	3		
ν_{SO}	18	65	69	103	
ν_{HSOH}	100	100	100	54	

[a] Present work.
[b] CCSD(T)/cc-pVQZ *ab initio* calculations from Ref. [6].
[c] CCSD(T)/cc-pV(T+*d*)Z *ab initio* calculations from Ref. [27].
[d] Values derived from gas-phase spectra. Numbers in parentheses are quoted uncertainties in units of the last digit given.
[e] Values derived from Ar-matrix spectra [6].
[f] Ref. [7].
[g] Ref. [10].
[h] Ref. [28].
[i] Ref. [1].
[j] Calculated from the transition moments and transition wavenumbers in Table 3 below.
[k] CCSD(T)/cc-pVQZ harmonic calculation [6].
[l] Derived from the CCSD(T)/cc-pV(T+*d*)Z harmonic-calculation results of Ref. [27].

In comparing the fundamental-level term values obtained in the present work with the previous theoretical values [6,27] (see Table 2), we should note that the *ab initio* calculations of Ref. [6] are made with the CCSD(T)/cc-pVQZ method in an all-electron treatment, the fundamental vibrational wavenumbers being determined from the *ab initio* data by perturbation methods. Denis [27] uses the CCSD(T)/cc-pV(T+*d*)Z *ab initio* method in the frozen-core approximation and determines the fundamental vibrational wavenumbers from the *ab initio* data by perturbation methods. In the present work, we produce an analytical representation of the PES based on CCSD(T)/aug-cc-pVTZ and CCSD(T)/aug-cc-pV(Q+*d*))Z *ab initio* data obtained in the frozen-core approximation, and we determine the fundamental vibrational wavenumbers in a variational approach. The various differences in the treatment all affect the computed wavenumbers, probably easily by several cm^{-1}. Therefore, the essentially perfect agreement with experiment obtained for the OH-stretch fundamental term value in the present work, and for the SH-stretch fundamental term value in Refs. [6] and [27], is probably fortuitous in all cases.

For the torsional splitting in the vibrational ground state (experimentally derived value: 0.00214 cm^{-1}; theoretical value from the present work: 0.00215 cm^{-1}), the excellent agreement between A(Q+*d*)Z* theory and experiment may also be to some extent accidental. Experimentally, the splitting for the SH fundamental level has an absolute value of (0.042 ± 0.002) cm^{-1} [10]; the sign cannot be determined. The theoretical value from the present work is -0.0775 cm^{-1} (Table 2). The less perfect agreement for this splitting could be caused by the fact that, owing to deficiencies of the PES, one of the split energy levels may come close to another level of the same symmetry, and the resulting interaction may then significantly change the splitting by amounts on the order of 0.1 cm^{-1}. However, on the positive side we correctly predict a larger absolute value for the splitting in the SH fundamental level relative to the vibrational ground state, in qualitative agreement with experiment. By contrast, Quack and Willeke [28] predict the SH-stretch-fundamental-level splitting to be 0.001672 cm^{-1}, a value slightly lower than that for the ground state. The fact that we obtain a negative value for the SH-stretch-fundamental-level splitting cannot be confirmed (or refuted) by experiment since, at the present time, experiment provides only the absolute value of this splitting. Our theoretical value of 0.0036 cm^{-1} for the OH-stretch-fundamental-level splitting is consistent with the experimental finding that this splitting is less than 0.01 cm^{-1}.

Along with the band centers we compute also the vibrational transition moments defined as

$$\bar{\mu}_{\rm if} = \sqrt{\sum_{\alpha=a,b,c} |\langle \Phi_{\rm vib}^{(f)} | \bar{\mu}_\alpha | \Phi_{\rm vib}^{(i)} \rangle|^2}, \quad (10)$$

where $|\Phi_{\rm vib}^{(w)}\rangle$, $w = i$ or f, are vibrational wavefunctions ($J = 0$), and $\bar{\mu}_\alpha$ is the component of $\bar{\mu}$ along the molecule-fixed $\alpha(=a, b, \text{and } c)$ axis. The matrix elements are generated using the vibrational eigenfunctions obtained from the variational calculations in conjunction with the *ab initio* A(Q+*d*)Z* potential energy and A(T+*d*)Z dipole moment surfaces.

The transition moments $\bar{\mu}_{\rm if}$ for the fundamental bands of HSOH and for the torsional overtones are compiled in Table 3, where we also list the individual matrix elements $\bar{\mu}_\alpha^{\rm if} = \langle \Phi_{\rm vib}^{(f)} | \bar{\mu}_\alpha | \Phi_{\rm vib}^{(i)} \rangle$, $\alpha = a, b, c$, from Eq. (10). As Supplementary material, we give a more extensive list of transition moments. The expectation values of the dipole moment components in the vibrational ground state are found to be significantly smaller than the corresponding *ab initio* equilibrium dipole moment values $\mu_a^{\rm eq}$, $\mu_b^{\rm eq}$, and $\mu_c^{\rm eq}$. As mentioned in Section 3.2, this is a consequence of the vibrational averaging. Consequently, the 'permanent dipole moment' components $\mu_a^{\rm eq}$, $\mu_b^{\rm eq}$, and $\mu_c^{\rm eq}$ cannot be used to estimate the line strengths [29] for rotational transitions of HSOH.

In Table 2, under the heading A(Q+*d*)Z*, we have included relative band intensities calculated from the transition moments and transition wavenumbers in Table 3. We obtain these relative intensities by calculating, for each fundamental band, the value of $\sum \tilde{\nu}_{\rm if} \bar{\mu}_{\rm if}^2$ (Table 3), where the sum is over the four torsional components of the band in question, and forming ratios of these quantities. These relative intensities can be roughly compared to those resulting from CCSD(T) calculations carried out at the cc-pVQZ [6] and cc-pV(T+*d*)Z [27] levels of theory, and to values obtained from the Ar-matrix spectrum [6]. These previous values are all included in Table 2. Concerning the comparison between the relative intensity results of the present work with the previous theoretical results [6,27], it should be noted that the cc-pVQZ [6] and cc-pV(T+*d*)Z [27] results are obtained under the assumption of all vibrational modes, including the torsion, being harmonic, and the intensities depending solely on the first derivatives of the DMS with respect to the vibrational coordinates. In computing the dipole moment matrix elements in Table 3 we, by contrast, use 'fully coupled', variationally determined wavefunctions and the complete DMS. We note in Table 2 that the relative intensities resulting from the cc-pVQZ [6] and cc-pV(T+*d*)Z [27] calculations are very similar but that the A(Q+*d*)Z* results of the present work deviate significantly from these previous results. We attribute the deviation to our more complete treatment of the nuclear motion, in particular of the torsion. To substantiate this assertion we have made a TROVE calculation which emulates the cc-pVQZ [6] and cc-pV(T+*d*)Z [27] calculations: In this calculation, we use the PES and DMS of the present work, but we describe the nuclear motion by means of a normal-coordinate Hamiltonian (using normal coordinates for all vibrational modes, including the torsion), and we truncate the potential energy expansion after the harmonic second-order terms and the dipole moment expansion after the linear terms. This simplified calculation gives relative-intensity ratios of $I(\nu_{\rm OH}):I(\nu_{\rm SH}):I(\nu_{\rm HOS}):I(\nu_{\rm OSH}):I(\nu_{\rm SO}):I(\nu_{\rm HSOH}) = 100:14:58:3:80:100$, in broad agreement with the cc-pVQZ [6] and cc-pV(T+*d*)Z [27] relative-intensity results in Table 2. The agreement demonstrates that the PES and DMS of the present work are similar to those of Refs. [6,27] and that the introduction, in TROVE, of anharmonicity, and of the correct double-minimum description of the torsional motion, significantly influences the relative intensities, leading to the A(Q+*d*)Z* results in Table 2. It is seen from the table that the most significant anharmonicity effect is a strengthening of the $\nu_{\rm HSOH}$ band relative to the other bands.

The comparison between the theoretical intensities, which are valid for an isolated molecule in the gas phase, and the Ar-matrix results should be made with some caution since the Ar-matrix intensities are believed to be rather uncertain; they may have uncertainties of 20–30% [31]. Also, it is known from experience [31] that the band intensities of a matrix spectrum sometimes deviate very strongly from those of the corresponding gas-phase spectrum, whereas the energy shifts relative to gas-phase spectra are normally small. The Ar-matrix results in Table 2 indicate that the $\nu_{\rm OH}$ and $\nu_{\rm HOS}$ bands are of comparable intensity, that the $\nu_{\rm SO}$ band is stronger than these two bands while the $\nu_{\rm SH}$ band is somewhat weaker, and that the $\nu_{\rm OSH}$ band is very weak. The A(Q+*d*)Z* prediction of the present work is, in fact, in keeping with these results, even though the predicted ratios of $I(\nu_{\rm OH})/I(\nu_{\rm SO}) = 16/18$ and $I(\nu_{\rm HOS})/I(\nu_{\rm SO}) = 13/18$ are much larger than the observed Ar-matrix ratios of 43/103 and 53/103, respectively. Whereas our A(Q+*d*)Z* calculation predicts the $\nu_{\rm OH}$ and $\nu_{\rm HOS}$ bands to be of comparable intensity (A(Q+*d*)Z* ratio 16:13, Ar-matrix ratio 43:53), the cc-pVQZ [6] and cc-pV(T+*d*)Z [27] calculations predict the $\nu_{\rm OH}$ band to be significantly stronger than the $\nu_{\rm HOS}$ band (predicted ratios 92:54 and 92:55, respectively). All three theoretical calculations predict the $\nu_{\rm SH}$ band to be about four times weaker than the $\nu_{\rm OH}$ band; this is in good agreement with a recent, accurate experimental determination (which will be discussed further in Section 5) of this intensity ratio from a gas-phase spectrum [7]. The Ar-matrix spectrum gives a $\nu_{\rm OH}/\nu_{\rm SH}$ intensity ratio of $43/8 \approx 5.4$, in broad agreement with the accurate gas-phase result. The $\nu_{\rm OSH}$ band is predicted to be quite weak by all theoretical calculations and, correspondingly, it is not observed in the Ar-matrix spectrum. The theoretical relative intensities in Table 2 all have in common that

Table 3
Band centers $\tilde{\nu}_{\rm if}$ (in cm^{-1}), vibrational transition moments $\bar{\mu}_{\rm if}$ (in D), and individual transition moment components ($\bar{\mu}_a^{\rm if}, \bar{\mu}_b^{\rm if}, \bar{\mu}_c^{\rm if}$) (in D) for selected vibrational transitions of HSOH.

Vibrational state[a]				Transition moments		
i	f	$\tilde{\nu}_{\rm if}$	$\bar{\mu}_{\rm if}$	$\bar{\mu}_a^{\rm if}$	$\bar{\mu}_b^{\rm if}$	$\bar{\mu}_c^{\rm if}$
0^+	0^+	0.000	0.699	0.040	0.698	
0^-	0^-	0.000	0.699	0.040	0.698	
0^+	0^-	0.002	1.297			−1.297
0^-	$\nu_{\rm HSOH}^+$	442.984	0.092			−0.092
0^+	$\nu_{\rm HSOH}^+$	442.986	0.527	−0.007	−0.527	
0^-	$\nu_{\rm HSOH}^-$	443.112	0.528	0.007	0.527	
0^+	$\nu_{\rm HSOH}^-$	443.114	0.092			0.092
0^-	$\nu_{\rm SO}^+$	759.951	0.028			0.028
0^+	$\nu_{\rm SO}^+$	759.953	0.173	−0.170	0.030	
0^-	$\nu_{\rm SO}^-$	760.006	0.173	0.170	−0.029	
0^+	$\nu_{\rm SO}^-$	760.008	0.028			−0.028
0^-	$2\nu_{\rm HSOH}^+$	843.130	0.134			−0.134
0^+	$2\nu_{\rm HSOH}^+$	843.132	0.052	−0.034	−0.039	
0^-	$2\nu_{\rm HSOH}^-$	846.267	0.051	−0.033	−0.038	
0^+	$2\nu_{\rm HSOH}^-$	846.269	0.135			−0.135
0^-	$\nu_{\rm OSH}^+$	1007.666	0.004			0.004
0^+	$\nu_{\rm OSH}^+$	1007.669	0.015	0.008	−0.012	
0^-	$\nu_{\rm OSH}^-$	1007.692	0.014	0.008	−0.012	
0^+	$\nu_{\rm OSH}^-$	1007.694	0.003			0.003
0^-	$\nu_{\rm HOS}^-$	1173.967	0.118	0.118	−0.007	
0^+	$\nu_{\rm HOS}^-$	1173.969	0.013			0.013
0^-	$\nu_{\rm HOS}^+$	1174.000	0.012			−0.012
0^+	$\nu_{\rm HOS}^+$	1174.002	0.117	−0.117	0.001	
0^-	$\nu_{\rm SH}^-$	2544.278	0.044	0.022	−0.038	
0^+	$\nu_{\rm SH}^-$	2544.280	0.000			
0^-	$\nu_{\rm SH}^+$	2544.356	0.000			
0^+	$\nu_{\rm SH}^+$	2544.358	0.044	0.022	−0.038	
0^-	$\nu_{\rm OH}^+$	3625.860	0.055			−0.055
0^+	$\nu_{\rm OH}^+$	3625.862	0.052	0.052	−0.005	
0^-	$\nu_{\rm OH}^-$	3625.863	0.052	−0.052	0.005	
0^+	$\nu_{\rm OH}^-$	3625.865	0.055			0.055

[a] A superscript − (+) signifies that the state in question has − (+) parity under the inversion operation E^* [29].

they predict the torsional fundamental band ν_{HSOH} to be the strongest fundamental band. This is in contrast to the Ar-matrix results where the ν_{SO} band is strongest which suggests that the intensity of the torsional band is strongly influenced by the presence of the Ar matrix.

5. The ν_{OH} and ν_{SH} fundamental bands

The rotation–torsion spectra associated with the transitions to the OH-stretch [7] and SH-stretch [7,10] fundamental levels have been experimentally recorded (see Fig. 4). Initial analysis [10] of the SH-stretch fundamental band has shown this band to be heavily perturbed. By contrast, the analogous spectra of the OH-stretch fundamental transition [6,7] appear largely "normal" and unperturbed. We discuss this in theoretical terms.

According to Table 3, the ν_{SH} band consists solely of *a*- and *b*-type transitions. In the formation of the ν_{OH} band the *a* and *c* components of the dipole moment are equally important, while the *b*-component contributes only very little.

Apart from this, we can make the rather trivial observation that the OH-stretching fundamental term value, at 3625 cm^{-1}, is significantly higher than the SH-stretching fundamental term value at 2538 cm^{-1}. At these energies, there is a significant density of excited torsional states and combination states involving bending and torsion. The wavefunctions describing such states at 3625 cm^{-1} involve more quanta of bending and torsional motion than those at 2538 cm^{-1}, so they have more nodes and are expected to produce smaller interaction matrix elements with the basis function for the OH-stretching fundamental level than the torsion/bending states around 2538 cm^{-1} do with the basis function for the SH-stretching fundamental. The 'pure' torsionally excited states found near the ν_{SH} state are $7\nu^{+}_{HSOH}$, $7\nu^{-}_{HSOH}$ $8\nu^{+}_{HSOH}$, and $8\nu^{-}_{HSOH}$ (at 2298.4, 2315.9, 2769.9, and 2730.3 cm^{-1}, respectively), whereas those closest to the ν_{OH} term value are the $9\nu^{+}_{HSOH}$, $9\nu^{-}_{HSOH}$, $10\nu^{+}_{HSOH}$, $10\nu^{-}_{HSOH}$ (at 3244.8, 3237.9, 3828.7, and 3823.7 cm^{-1}, respectively). Here, a superscript −(+) signifies −(+) parity under the inversion operation E^{*} [29].

Furthermore, Fig. 1 of Ref. [9] suggests that in the PES of HSOH, the SH-stretching mode is more strongly coupled to the torsion than the OH-stretching mode. The optimized value of r_{SH} as a function of a torsional angle shows a distinct variation while the analogous value of r_{OH} varies much less. In the left display of Fig. 5 we show the OH-stretch and SH-stretch harmonic vibrational wavenumbers ω_{OH} and ω_{SH}, respectively, computed from the A(Q+*d*)Z* PES at the optimized geometries displayed in Fig. 1 of Ref. [9]. We see that ω_{SH} varies essentially more with the torsional angle than does ω_{OH}; this is in keeping with our observation that the coupling between the SH-stretching mode and the torsional mode is larger than that between the OH-stretching mode and the torsional mode. The shaded areas on this figure show the τ_{HSOH}-inter-

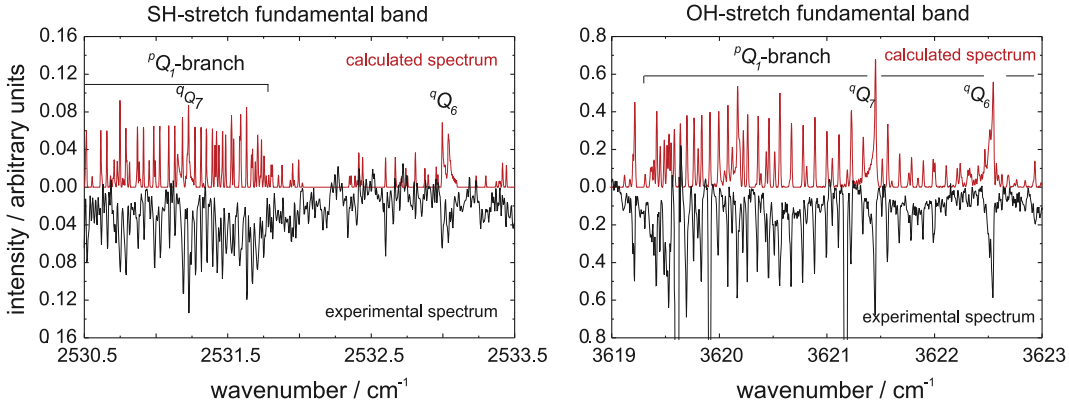

Fig. 4. Comparison of the $^{p}Q_{1}$-branch regions of the ν_{OH} and ν_{SH} fundamental stretching bands. The experimental spectra have been recorded using the Bruker IFS 120 HR Fourier transform spectrometer at the University of Wuppertal [6,7,10]. The calculated spectra are obtained at an absolute temperature of 300 K and based on molecular constants from the experimental data analyses given in Refs. [7,10]. The spectrum of the ν_{SH} band is displayed with an ordinate scale magnified 5× relative to that of the ν_{OH} band.

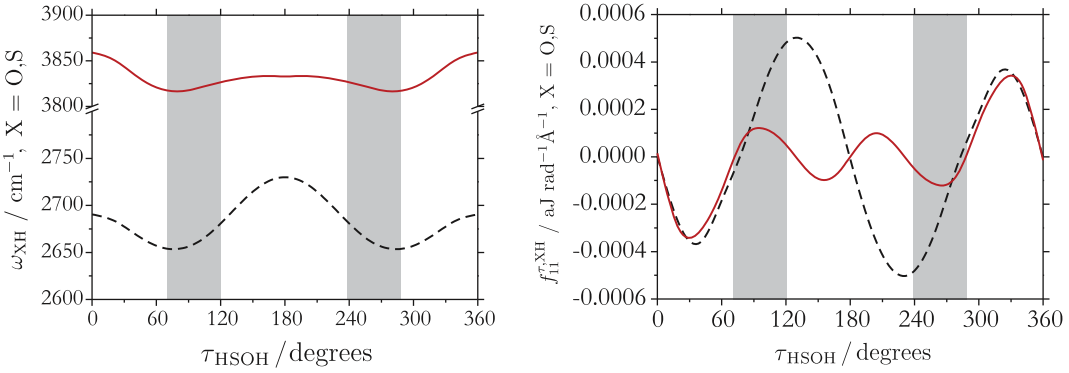

Fig. 5. (left) Harmonic vibrational wavenumbers ω_{OH} (solid curve) and ω_{SH} (dashed curve), computed from the A(Q+*d*)Z* PES at the optimized geometries displayed in Fig. 1 of Ref. [9]. (right) Second derivatives $f_{11}^{\tau,XH} = \partial^{2}V/\partial r_{XH}\partial\tau_{HSOH}$, X = O (solid curve) and S (dashed curve), computed at the optimized geometries displayed in Fig. 1 of Ref. [9]. The shaded areas in the two displays show the τ_{HSOH}-intervals where the vibrational-ground-state torsional wavefunction has an amplitude of more than 50% of the maximum amplitude.

vals where the vibrational-ground-state torsional wavefunction has an amplitude of more than 50% of the maximum amplitude. The right display of Fig. 5 shows the values of the 'mixed' second derivatives $f_{11}^{\tau,XH} = \partial^2 V/\partial r_{XH}\partial\tau_{HSOH}$, X = S and O, computed at the optimized geometries displayed in Fig. 1 of Ref. [9]. The mixed second derivatives confirm that the strongest coupling is found between the torsion and the SH-stretching mode.

As mentioned above, it has been found experimentally [7] that ν_{SH} fundamental band is 4–5 times weaker than the ν_{OH} fundamental band. This is borne out by Fig. 4 where we compare the experimentally measured ${}^pQ_1$ branches of the ν_{OH} and ν_{SH} absorption bands [7,10]. The ratio $I(\nu_{OH})/I(\nu_{SH})$ of the ν_{OH} and ν_{SH} integrated band intensities is determined experimentally [7] as 4.4 ± 0.8. According to the theoretical transition moment values from Table 3 (and the ratio of the band center wavenumbers), the ν_{OH} band is estimated to be about 4.3 times stronger than the ν_{SH} band, in good agreement with the experimental findings. The CCSD(T)/cc-pVQZ calculation from Ref. [6] gives a corresponding ratio of $92/22 \approx 4.2$ (see Table 2).

6. Summary and conclusion

We have used the coupled-cluster CCSD(T) *ab initio* method to generate a high-level potential energy surface, together with a high-level dipole moment surface, for the electronic ground state of HSOH. In the calculation of the potential energy surface, the *ab initio* points characterizing the surface in the low-energy region (up to 12 000 cm^{-1} above equilibrium) are computed using a very large basis (cc-pVQZ for H, aug-cc-pVQZ for O, and aug-cc-pV(Q+*d*)Z for S). Points in the energy region between 12 000 and 20 000 cm^{-1} above equilibrium are calculated with aug-cc-pVTZ basis sets for all nuclei. The two *ab initio* data sets were combined to produce an analytical representation of the PES as explained in Section 3. The dipole moment components were calculated by the CCSD(T)/A(T+*d*)Z method and fitted to analytical functions as explained in Section 3.2.

The analytical representations of the potential-energy and dipole-moment surfaces were used as input for the program TROVE [14] in order to calculate the vibrational energies and transition moments for selected vibrational transitions of HSOH. We find that for HSOH, the transition moment values depend significantly on the theoretical description of the nuclear motion. With our double-minimum description of the torsional motion and anharmonic treatment of the other vibrational modes, we obtain relative intensities for the fundamental bands (Table 2) that differ considerably from the results of the harmonic calculations reported in Refs. [6,27].

As discussed above, the theoretical results of the present work are generally in good agreement with the experimental data available for HSOH. The theoretical results allow us to explain, at least tentatively, extensive perturbations recently found experimentally in the SH-stretch fundamental band of HSOH. The present calculations suggest that the torsional splittings in the fundamental levels ν_{SH}, ν_{HOS}, ν_{OSH}, ν_{SO}, and ν_{HSOH} are significantly larger than that in the vibrational ground state (Table 2). As discussed above, this is consistent with the experimental observation of the SH-stretch fundamental band [7,10]. The previous MP2/aug-cc-pVTZ calculations from Ref. [28] predicted a similarly large increase of the splitting upon excitation of the ν_{HSOH} mode, but gave splittings for the other fundamental levels which are comparable to that of the vibrational ground state (Table 2). We plan an experimental study of the SO-stretch fundamental band to clarify this issue.

Acknowledgments

We are grateful to Prof. Helge Willner for helpful discussions. We acknowledge support from the European Commission (contract no. MRTN-CT-2004-512202 "Quantitative Spectroscopy for Atmospheric and Astrophysical Research" (QUASAAR)).

Appendix A. Supplementary data

Supplementary data for this article are available on ScienceDirect (www.sciencedirect.com) and as part of the Ohio State University Molecular Spectroscopy Archives (http://library.osu.edu/sites/msa/jmsa_hp.htm).

References

[1] G. Winnewisser, F. Lewen, S. Thorwirth, M. Behnke, J. Hahn, J. Gauss, E. Herbst, Chem. Eur. J. 9 (2003) 5501–5510.
[2] M. Behnke, J. Suhr, S. Thorwirth, F. Lewen, H. Lichau, J. Hahn, J. Gauss, K.M.T. Yamada, G. Winnewisser, J. Mol. Spectrosc. 221 (2003) 121–126.
[3] K.M.T. Yamada, G. Winnewisser, P. Jensen, J. Mol. Struct. 695–696 (2004) 323–337.
[4] S. Brünken, M. Behnke, S. Thorwirth, K.M.T. Yamada, T.F. Giesen, F. Lewen, J. Hahn, G. Winnewisser, J. Mol. Struct. 742 (2005) 237–242.
[5] O. Baum, S. Esser, N. Gierse, S. Brünken, F. Lewen, J. Hahn, J. Gauss, S. Schlemmer, T.F. Giesen, J. Mol. Struct. 795 (2006) 256–262.
[6] H. Beckers, S. Esser, T. Metzroth, M. Behnke, H. Willner, J. Gauss, J. Hahn, Chem. Eur. J. 12 (2006) 832–844.
[7] O. Baum, T.F. Giesen, S. Schlemmer, J. Mol. Spectrosc. 247 (2007) 25–29.
[8] O. Baum, M. Koerber, O. Ricken, G. Winnewisser, S.N. Yurchenko, S. Schlemmer, K.M.T. Yamada, T.F. Giesen, J. Chem. Phys. 129 (2008) 224312.
[9] R.I. Ovsyannikov, V.V. Melnikov, W. Thiel, P. Jensen, O. Baum, T.F. Giesen, S.N. Yurchenko, J. Chem. Phys. 129 (2008) 154314.
[10] O. Baum, Ph.D. dissertation, University of Cologne, 2008.
[11] K.M.T. Yamada, P. Jensen, S.C. Ross, O. Baum, T.F. Giesen, S. Schlemmer, J. Mol. Struct. 927 (2009) 96–100.
[12] J.T. Hougen, Can. J. Phys. 62 (1984) 1392–1402.
[13] J.T. Hougen, B. DeKoven, J. Mol. Spectrosc. 98 (1983) 375–391.
[14] S.N. Yurchenko, W. Thiel, P. Jensen, J. Mol. Spectrosc. 245 (2007) 126–140.
[15] J.T. Hougen, P.R. Bunker, J.W.C. Johns, J. Mol. Spectrosc. 34 (1970) 136–172.
[16] P.R. Bunker, B.M. Landsberg, J. Mol. Spectrosc. 67 (1977) 374–385.
[17] MOLPRO, version 2002.3 and 2002.6, a package of *ab initio* programs written by H.-J. Werner, P.J. Knowles, with contributions from R.D. Amos, A. Bernhardsson, A. Berning et al.
[18] C. Hampel, K. Peterson and H.-J. Werner, Chem. Phys. Lett. 190 (1992) 1-12 and references therein. The program to compute the perturbative triples corrections has been developed by M.J.O. Deegan and P.J. Knowles, ibid 227 (1994) 321–326.
[19] G.D. Purvis, R.J. Bartlett, J. Chem. Phys. 76 (1982) 1910–1918.
[20] M. Urban, J. Noga, S.J. Cole, R.J. Bartlett, J. Chem. Phys. 83 (1985) 4041–4046.
[21] K. Raghavachari, G.W. Trucks, J.A. Pople, M. Head-Gordon, Chem. Phys. Lett. 157 (1989) 479–483.
[22] T.H. Dunning, J. Chem. Phys. 90 (1989) 1007–1023.
[23] D.E. Woon, T.H. Dunning, J. Chem. Phys. 98 (1993) 1358–1371.
[24] R.A. Kendall, T.H. Dunning, R.J. Harrison, J. Chem. Phys. 96 (1992) 6796–6806.
[25] A.K. Wilson, T.H. Dunning, J. Chem. Phys. 119 (2003) 11712–11714.
[26] S.N. Yurchenko, H. Lin, J.J. Zheng, P. Jensen, W. Thiel, J. Chem. Phys. 123 (2005) 134308.
[27] P.A. Denis, Mol. Phys. 106 (2008) 2557–2567.
[28] M. Quack, M. Willeke, Helv. Chim. Acta 86 (2003) 1641–1652.
[29] P.R. Bunker, P. Jensen, Molecular Symmetry and spectroscopy, second ed., NRC Research Press, Ottawa, 1998.
[30] J.W. Cooley, Math. Comp. 15 (1961) 363–374.
[31] H. Willner, private communication.